Multi-temporal terrestrial photogrammetry for landslide monitoring

J. Travelletti, J.-P. Malet, J. Schmittbuhl, R. Toussaint, M. Bastard
Institut de Physique du Globe de Strasbourg, CNRS UMR 7516, University of Strasbourg (EOST), 5 rue René Descartes, 67084 Strasbourg Cedex, France. E-mail : julien.travelletti@unistra.fr

C. Delacourt
Université Européenne de Bretagne, Institut Universitaire Européen de la Mer, CNRS UMR 6538, University of Brest, Brest, France.

P. Allemand
Laboratoire des Sciences de la Terre, Université Lyon et Ecole Normale Supérieure, Lyon, France

D.B. van Dam
Faculty of Geosciences, Department of Physical Geography, Utrecht University, Utrecht, Netherlands.

ABSTRACT: The objective of this work is to present an inexpensive method to monitor the displacement pattern of slow-moving landslides from terrestrial oblique optical images analyzed with a Digital Image Correlation (DIC) technique. The performance of the method is evaluated on the Super-Sauze landslide (South French Alps). The image monitoring system consists in a low-cost optical camera installed on a concrete pillar located on a stable crest in front of the landslide and controlled by a datalogger.
To estimate the planimetric ground displacement that occurred between several images acquired over the same area at several different times, a cross-correlation algorithm using a multi-resolution approach is used. The correlation is first calculated in the image plane of the camera in terms of pixel displacements and direction. Then, a method based on the collinearity equations to orthorectify and georeference the displacements field in the local coordinate system with a high resolution DEM is used.
In the image plane of the camera, the displacement pattern is clearly identified. The maximum of displacement amplitudes is identified in spring 2008 after important rainfalls and snow melting. The amplitude and direction of pixel displacements indicate displacement fields with different kinematics between the upper and the lower part of the landslide. The total amplitude of displacements decreases from the upper part (10.5 m in 4 days) to the lower part of the mudslide (1.1 m in 4 days). The normal landslide activity is recovered with an average daily velocity of about 0.01 m.day^{-1} between end of July and October 2008. Horizontal cumulated displacements for 2008 reach 38 m for the upper part and 7 m for the lower part.
If the landslide is mainly translational without excessive changes in elevation, the same DEM can be used to estimate the displacements in the local coordinate system. The changes in meteorological conditions (snow, clouds, rain storm), in surface conditions (important ground deformations) and in illumination conditions are the main limitations that have to be taken into account to integrate this technique in an early warning system.

1 INTRODUCTION

The kinematics characterization of landslides is a prior to understand landslide mechanism for hazards and risk assessments. Because such natural processes are very sensitive to climatic conditions, their behavior is permanently changing in time and in space, thus making the characterization of landslide kinematics difficult with conventional and punctual geodetic measurements like tacheometry, extensometry and GPS surveys. The application of optical correlation methods is thus particularly efficient for monitoring the spatial heterogeneity of landslide displacements (Kääb, 2002; Casson et al., 2003; Delacourt et al., 2007; LePrince et al., 2008). The performance of the correlation technique on aerial (eg. IGN) and high-resolution satellite images (eg. SPOT, QuickBird, OrbView, EROS) is widely demonstrated for landslide monitoring (Casson et al., 2003; Delacourt et al., 2004; LePrince et al., 2008). However, the acquisition frequency and the spatial resolution of aerial and satellite images are some typical parameters that cannot be controlled by the user. These drawbacks can be very problematic in function of the size and the dynamics of the landslide. Correlation of optical terrestrial images is a good complementary method to aerial and satellite imaging and classical landslide monitoring techniques. Optical terrestrial images can be acquired from a fixed location, generally in front of the landslide with a high resolution and a frequency adapted to the landslide velocity. The images are systematically acquired in exactly the same geometry.

Terrestrial digital images are commonly used to generate accurate Digital Elevation Models (DEMs) for 3D morphological analysis and ortho-rectification of images (Cardenal et al., 2008). The camera system is generally installed for a short period and removed after each acquisition. Therefore only a few examples demonstrated its potential for continuous monitoring of landslides kinematics (eg. Delacourt et al., 2007). This work precisely attempts to present a low-cost permanent monitoring system to characterize the displacement pattern of slow moving landslides from terrestrial multi-temporal optical images acquired in the Super-Sauze mudslide. The Digital Image Correlation (DIC) techniques, the georeferencing procedure and the associated accuracy are explained. Finally the results of the landslide displacements in the image plane and in the local reference system for the monitoring period of 2008 are presented and discussed.

2 EXPERIMENTAL SITE: THE SUPER-SAUZE MUDSLIDE

The Super Sauze mudslide is located in the Callovo-Oxfordian black marls of the Southern French Alps (Alpes-de-Haute-Provence, France). Its extents over a distance of 920 m between an elevation of 2105 m at the crown and 1736 m at the toe with an average width of 150 m and a average slope of 25° (Figure 1). Last estimations of the total volume is evaluated at 560,000 m^3 (Travelletti & Malet, submitted).
The mudslide is gradually covering a torrential stream located downstream with typical range of velocity between 1 to 3 $cm.d^{-1}$ and acceleration peak until 40 $cm.d^{-1}$ in the spring season (Malet et al., 2002). The kinematics of the landslides is currently monitored by DGPS survey, terrestrial laser scanning and the permanent camera monitoring system.

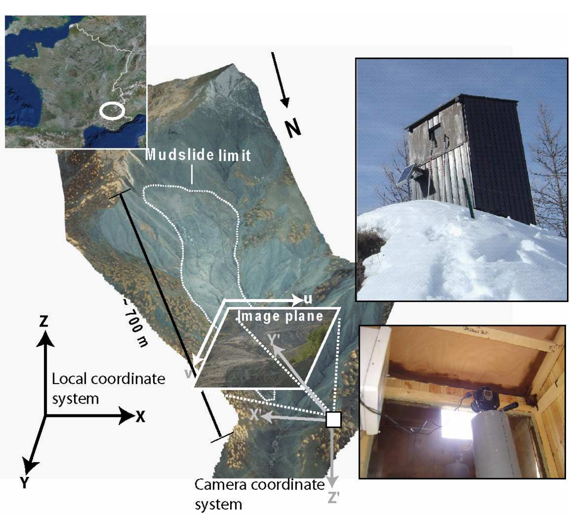

Figure 1.View of the Super-Sauze mudslide, the camera monitoring system and the different coordinates system involved in the georeferencing procedure.

3 METHODOLOGY

3.1 *Instrumentation*

The monitoring system consists of a low-cost D70 Nikon non metric reflex digital camera (about 1500 €) installed on a concrete pillar located on a stable crest in front of the mudslide at a distance of 300 m from the lower part and 900 m from the upper part of the mudslide (Figure 1). The acquisition system is controlled by a datalogger (CR10) and the power is provided by a 40 W solar panel. The characteristics of the acquisitions are presented in Table 1. The focused of the camera lens is set to manual. The frequency of acquisition is four days. An acquisition consists in four photographs registered at 11:00 a.m., 12:00 p.m., 13:00 p.m. and 14:00 p.m in order to get at least one image taken during good meteorological conditions. Each photograph (6 Mb) is stored in a native file format without any loss of information.

Table 1. Camera acquisitions characteristics

Type of Camera	Single-lens reflex digital camera
Effective Pixels	6.1 million
Image Sensor	RGB CCD, 23.7 x 15.6 mm
Image Size	3008 x 2000
Principal point	(1504 ,1000)
Sensitivity	400 iso
Focal length	52 mm
Shutter speed	1/8000
Storage Media	CompactFlash™ (CF) Card
Storage System	NEF (RAW)

3.2 *Processing*

3.2.1 *Digital Image Correlation (DIC)*

Different terminologies exist in the literature to designate methods searching for the greatest correspondence between two signals like Particle Image Velocimetry (PIV), Correlation Image velocimetry (CIV) and Digital Image Correlation (DIC). DIC is the most used terminology for applications in geosciences.

The correlation principle is to recognize identical intensity distribution patterns on a reference image and a second image after displacements. Most of DIC techniques are based on a maximization of a normalized cross-correlation function due to the reliability and the simplicity of the method (Lewis, 1995; Debella-Gilo and Kääb, in press). The function is solved either in the spatial domain or in the frequency domain by using FFT algorithm (Hild et al. 1999). The normalized cross-correlation function for two discretely sampled images is defined as:

$$\Phi(u,v) = \frac{\sum_{x,y}[f(x,y)-\bar{f}_{u,v}][t(x-u,y-v)-\bar{t}]}{\left\{\sum_{x,y}[f(x,y)-\overline{f_{u,v}}]^2\sum_{x,y}(t(x-u,y-v)-\bar{t})^2\right\}^{0.5}} \quad (1)$$

f contains the image intensity distribution of the reference image. $\bar{f}_{u,v}$ is the mean of $f(x,y)$ in the region under the feature. $\bar{t}$ is the mean value of the correlation window. $\Phi(u, v)$ is the cross-correlation function. If $\Phi(u, v)$ is equal to 0, there is no relationship between the matching entities. If $\Phi_{fg}(u, v)$ is equal to 1, the matching is maximal. The Euclidean distance between the coordinates of the reference point and the matching points represents the displacements magnitude in the image plane. By changing the zone of interest, it is then possible to determine displacements at various positions inside the images. In this study, the use of a multi-resolution correlation algorithm with subpixel accuracy is motivated by the necessity:

- to minimize incoherent results due to changes in landslide surface aspect (soil moisture changes, soil surface weathering) and changes in illumination
- to identify and characterize heterogeneous distributed displacement fields.

The correlation algorithm is based on:

- successive degradations of image resolution for changing the physical size of the interest zone. The correlator starts at the lowest resolution image for determining global displacements, then the location of the maximum cross-correlation is used as a start point for the next correlation with a higher resolution to determine local displacements.
- correlation of gradient values by using an edge detection algorithm (Sobel or Prewitt operators), applied on the images to identify object texture (Chambon et al., 2003).

The sub-pixel displacement is computed using an iterative procedure in order to find the maximum of the correlation function interpolated with a bi-parabolic formula between the pixel centers. The maximisation procedure is based on the simplex method (Press et al., 1997). For a thorough description of the multi-resolution correlator and the sub-pixel computation, see Bastard (2009) and Chambon (2003).

The correlation algorithm and the pre and post-processing steps are written in C++ and Matlab programming languages.

3.2.2 Georeferencing

Because the pixel resolution depends on the distance between the landslide and the camera and on the terrain orientation relative to the line of sight of the camera, the displacements field determined in the image plane cannot be directly interpreted in metric displacements. However, a quantitative analysis is possible if a DEM is available to relate two-dimensional pixel positions in the image plane to three-dimensional points in the local coordinate system. The DEMs are usually produced with stereoscopic pair of images taken at the same time (Mikhail et al., 2001; Casson et al., 2003). This method required the installation of at least two terrestrial cameras at different viewpoints. In order to overcome this problem, a DEM interpolated from airborne LiDAR data set (0.25 m mesh size with a planimetry accuracy of 0.15 m and an elevation accuracy of 0.10 m) is used assuming that the landslide morphology remains constant with time. This strong hypothesis will obviously affect the accuracy of the displacements converted in the local coordinate system. However, it will be further demonstrated that this method is still a good estimation.

The external parameters of the camera are first determined. Then a projective transformation in the image plane is applied on the DEM to allocate a 3D position at each 2D pixel coordinates.

3.2.2.1 External parameters of the camera

The relationship between the image coordinates (u,v) and the local coordinates system (X,Y,Z) is given by the classical form of the collinearity equations (Mikhail et al., 2001):

$$u = u_0 - f\,\frac{m_{11}(X-X_C)+m_{12}(Y-Y_C)+m_{13}(Z-Z_C)}{m_{31}(X-X_C)+m_{32}(Y-Y_C)+m_{33}(Z-Z_C)} \quad (2)$$
$$v = v_0 - f\,\frac{m_{21}(X-X_C)+m_{22}(Y-Y_C)+m_{23}(Z-Z_C)}{m_{31}(X-X_C)+m_{32}(Y-Y_C)+m_{33}(Z-Z_C)}$$

The origin of the image plane system is located at the upper left corner of the image (Figure 1). (u_0,v_0) are the coordinates of the principal point. (X_C,Y_C,Z_C) are the coordinates referring to the camera station in the local coordinate system. f is the focal length of the camera. The X-axis is defined along the W-E direction and the Y-axis along the S-N direction in the local coordinate system. The Z-axis is the elevation perpendicular to the plane (X,Y). m_{ij} are the components of the rotation matrix **M** that defines the external parameters of the camera. **M** is constructing by using three sequential rotation angles: ω around the X-axis, φ around the once-rotated Y-axis and κ around the twice-rotated Z-axis:

$$\mathbf{M} = \begin{pmatrix} \cos\varphi\cos\kappa & \cos\omega\sin\kappa+\sin\omega\sin\varphi\cos\kappa & \sin\omega\sin\kappa-\cos\omega\sin\varphi\cos\kappa \\ -\cos\varphi\sin\kappa & \cos\omega\cos\kappa-\sin\omega\sin\varphi\sin\kappa & \sin\omega\sin\kappa+\cos\omega\sin\varphi\sin\kappa \\ \sin\varphi & \sin\omega\cos\varphi & \cos\omega\cos\varphi \end{pmatrix} \quad (3)$$

The estimation of the three independent angles involved in the rotation matrix is the most sensitive part in camera calibration (Mikhail et al., 2001). In order to compute the external parameters of the camera, Ground Control Points (GCPs) identified both in the image plane and in the local coordinate system are used as input data for a self calibration. 95 pairs of GCPs distributed on the image plane and in the local reference system were measured using a Differential Global Positioning System (DGPS) (Fig 2). The GCPs are measured in the local coordinate system with an average 3D accuracy of 0.02 m and a standard deviation of 0.01 m. The GCPs coordinates (u_i,v_i) in the image plane are determined by manual picking with an estimated accuracy of about 2 pixels. Among the 95 GCPs, 45 are used to compute the rotation matrix **M** and 40 are kept for the accuracy analysis. Equ. 2 is then used to obtain the calculated image coordinates of the GCPs using the ground positions of the GCPs. A least mean squares minimization between observed and calculated GCPs in the image plane using Singular Value Decomposition allows to determine the rotational matrix **M** that satisfies the system of Equ. 2 (Heikkilä and Silven, 1997). The camera location measured by DGPS, the focal length (constant for each acquisition) and the central points coordinates (u_0,v_0) provided by the manufacturer are included in the least mean squares minimization to better constrain the rotation matrix computation.

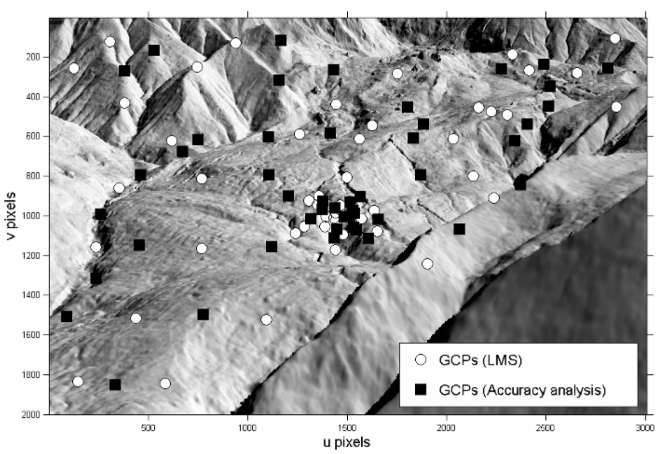

Figure 2. Location of the GCPs in a synthetic image for the Least Mean squared Minimization (LMS) and for the accuracy analysis. The synthetic image is produced by interpolation of the hillshade values of the DEM projected in the image plane.

3.2.2.2 Projection of the DEM in the image plane

Once the rotation matrix **M** is determined, Equ. 2 is applied on the whole DEM. In order to avoid the projection of duplicate points in the same position in the image plane, the points of the DEM invisible from the camera view point C (X_C, Y_C, Z_C) are identified. This step is computed using the sightline method (Fisher, 1994; Franklin and Ray, 1994). The sightline $\boldsymbol{S}$ is defined as the straight line from the camera location (X_C,Y_C,Z_C) to the position P (X,Y,Z) located in the gridded DEM. $\boldsymbol{S}$ is defined as follows:

$$\begin{bmatrix} s_x \\ s_y \\ s_z \end{bmatrix} = \begin{bmatrix} x \\ y \\ z \end{bmatrix} + k \begin{bmatrix} x - x_c \\ y - y_c \\ z - z_c \end{bmatrix} \quad , k \in IR \quad (4)$$

If a point of the sightline between the camera location C and the position P goes below the DEM surface ($Z < Z_{DEM}$), P is invisible from the camera location.

Once the visible points of the DEM are projected in the image plane, a linear interpolation is used to associate the X,Y,Z coordinates for each pixel location (u,v) of the image plane. The georeferencing in the local coordinate system of the displacement field determined with the DIC technique can be then applied.

4 ACCURACY ANALYSIS

4.1 Accuracy of the multi-resolution correlator

The accuracy of the multi-resolution correlator was assessed by applying homogeneous synthetic displacement fields on a real image as suggested by Chambon et al. (2003). Three different levels of gaussian noise are added on the synthetic displaced image. The mean Gaussian noise is fixed to null and the variance σ_n^2 is fixed to 10^{-4}, 10^{-3} and 10^{-2} respectively. The DIC is then applied on the real image and the synthetic displaced image. The difference between the calculated displacements and the imposed displacements allow to determine the accuracy of the correlator algorithm (Figure 3). As observed by Hild et al. (1999), the accuracy of the algorithm mainly depends on the pixel fraction of the displacement. For fifteen tests realized with a magnitude of imposed displacements between 1 to 23 pixels, the accuracy of the correlator varies between ± 0.5 pixels for the highest degree of noise and ± 0.1 pixels for the lowest degree of noise.

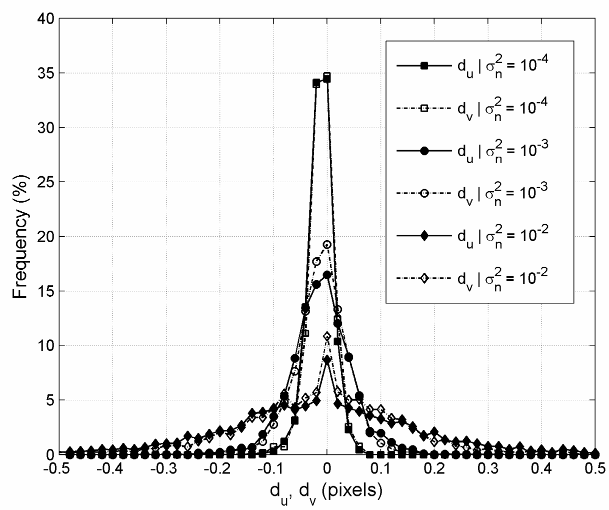

Figure 3. Accuracy of the hierarchical correlator in u and v directions in function of different levels of Gaussian noise (σ_n^2).

4.2 Influence of the image resolution

The effective pixel size is a limiting parameter for the correlation accuracy (Figure 4). The pixel size depends on (i) the distance between the terrain surface and the camera and (ii) the angle of incidence which is defined as the complementary angle between the line of sight of the camera and the normal terrain surface. The pixel size determines the minimum theoretical displacement that can be detected by the DIC technique for pixel-level correlation.

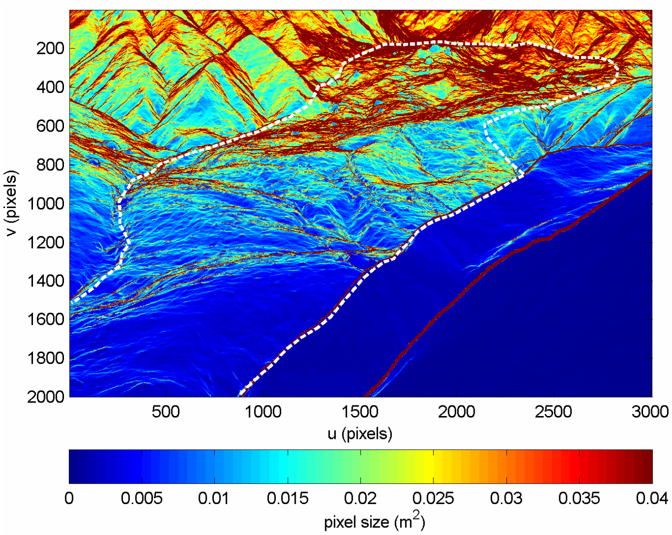

Figure 4. Effective pixel size

The pixel size varies from 1.10^{-2} m^2 in the lower part to 3.10^{-2} m^2 in the upper part of the landslide. Minimum displacements for pixel-level correlation in *u* and *v*-direction of 0.15 m and 0.08 m in the lower part of the landslide and 0.30 and 0.10 m in the upper part are found (Figure 5A, B). Below these displacement thresholds, the accuracy mainly depends on the sub-pixel correlation accuracy.

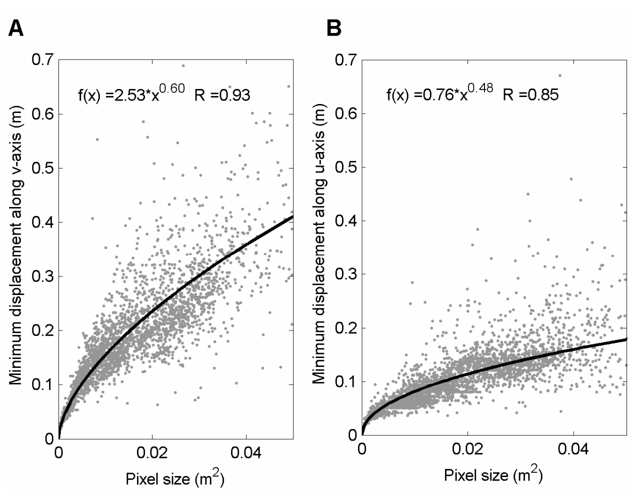

Figure 5. Minimum displacements for pixel-level correlation A) along v and B) along u-axis in function of the pixel size

4.3 Accuracy of the external parameters

The 40 GCPs not introduced in the minimization processes are used to evaluate the absolute accuracy of the rotational matrix **M** (Equ. 3). The shift between the projected and the observed GCPs positions in the image plane is determined (Figure 6). A mean shift error of -0.20 pixel and -0.08 pixel with a standard deviation of 1.59 pixel and 1.51 pixels in *u* and *v* direction respectively is found (Table 2). Because the standard deviation is close to the accuracy of the GCPs picking, the solution is judged acceptable.

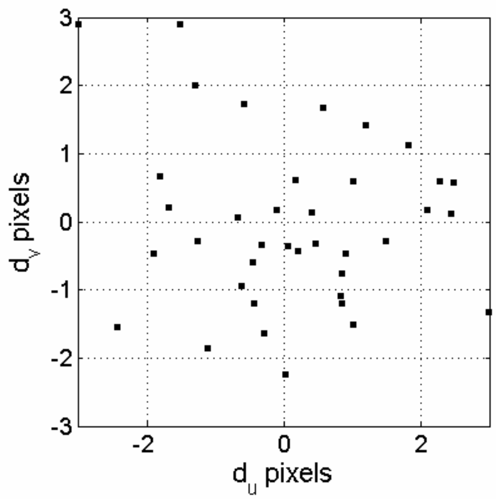

Figure 6. Residual *du* and *dv* misfits between projected and observed GCPs after the minimization.

To control the overall quality of the transformation, a synthetic image of the landslide is reproduced by interpolating the shaded relief value computed in the DEM. Regarding the accuracy of the transformation matrix and the realism of the synthetic image, the results are satisfying (Figure 2; Figure 6).
Slight external parameters changes (movements of the camera) can lead to the occurrence of a homogeneous component in the calculated displacements field in the image plane. These artefacts can be corrected with an automatic routine by removal of the misfit determined in the stable part of the mudslide on the whole computed displacements. Then the accuracy of the displacement in the image plane is assessed by a null test over stable areas by looking at the residual (Casson et al., 2005).

4.4 Accuracy of the georeferencing

The accuracy of the georeferencing in the local coordinate system is calculated by comparing the back-projected GCPs with their DGPS position located in the stable part of the landslide where no geomorphic change occurred. The absolute accuracy in *X, Y* and *Z* coordinate are presented in Table 2.

Table 2. Mean μ and standard deviation σ of the absolute accuracy for the projection in the image plane and the back-projection in the local coordinate system

Image plane (n=40)	μ (pixels)	σ (pixels)
u	0.20	1.59
v	-0.08	1.51
Local coordinate system (n=11)	μ (m)	σ (m)
X	0.07	0.41
Y	-0.13	0.53
Z	0.01	0.29

5 RESULTS

5.1 Displacement field in the image plane

41 pairs of images are correlated for the year 2008. The residual misfit after correction of slight movements of the camera is evaluated at about 1 pixel on average and corresponds to an estimation of the displacement accuracy in the image plane.
Loss of coherence is observed in areas where changes of surface texture are too important. Consequently, some points present unreliable displacements characterized with an amplitude and a direction very different from the neighboring points (eg. displacements going upslope). Such points can be thus easily detected and removed (Casson et al. 2005). Aberrant results are also removed according to their correlation coefficient. A correlation threshold coefficient has been fixed to 0.75. Below it, displacements are not considered reliable.

In spring 2008, persistent rainfalls and a fast melting of the snow cover were the main causes of an important acceleration. This acceleration could be measured by the DIC technique from the 20th of May when the snow cover on the landslide completely melt. Figure 7 shows the displacement field in the image plane the 20th of May and the cumulated displacements for 9 profiles crossing the landslide between the 20th of May and the 25th June. The profiles at positions *v* of 200 and 400 clearly point out the stable crest in the center of the upper part (u = 2000 and v = 400) where cumulated displacements are null. On both sides of the crest, the largest pixels velocities are observed. They reach 6 pixels.day^{-1} at the peak of the acceleration at the beginning of June 2008. In one month, cumulated displacements reach 110 pixels in the upper part. Figure 8B shows the cumulated displacement of fours points (Points 1, 2, 3 and 4) respectively located in the upper, medium, lower and stable part of the mudslide. The major mudslide displacements occur in the spring season when the ground water level reached its maximum level. Then, the normal landslide activity is recovered with an average daily velocity of 0 to 1 pixel.day^{-1}.

Figure 7. Displacement field computed at the 20th May and cumulated displacements over the acceleration period of the mudslide. The location of the points 1, 2, 3 and 4 are referring to Figure 8.

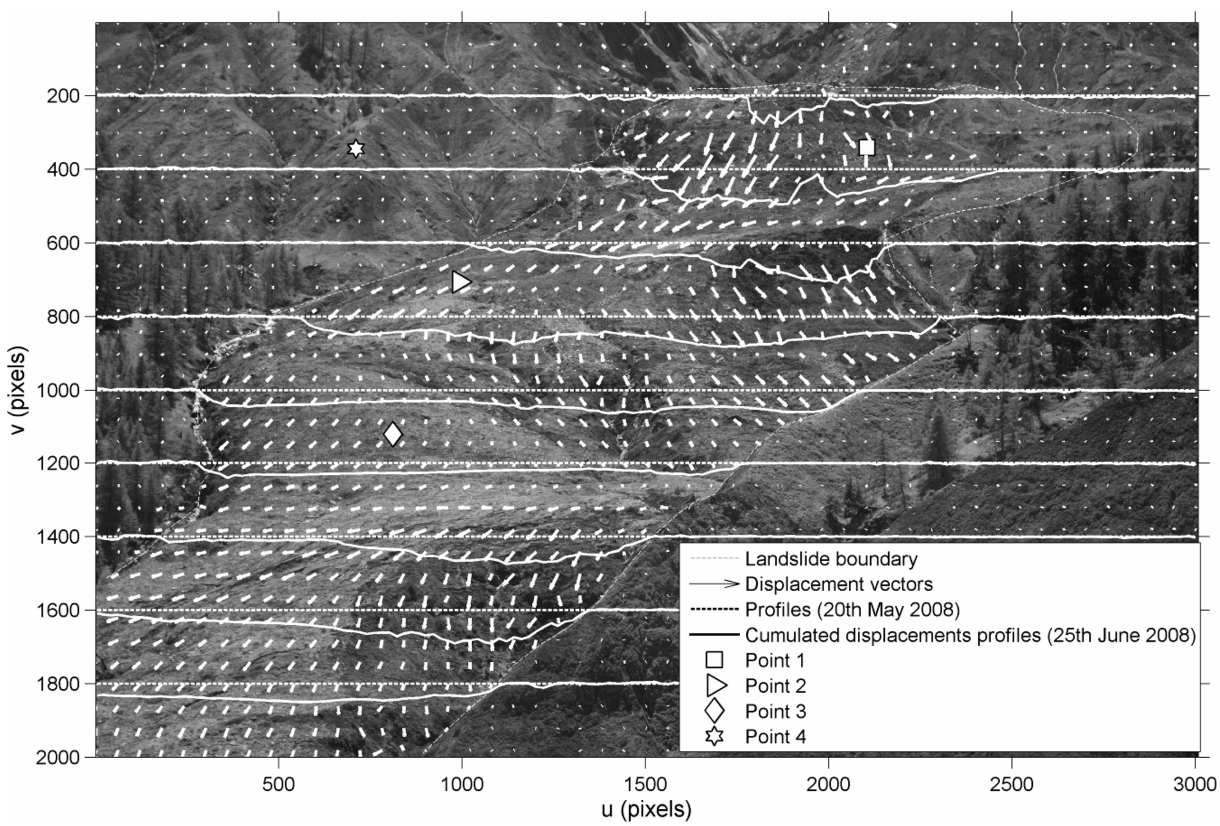

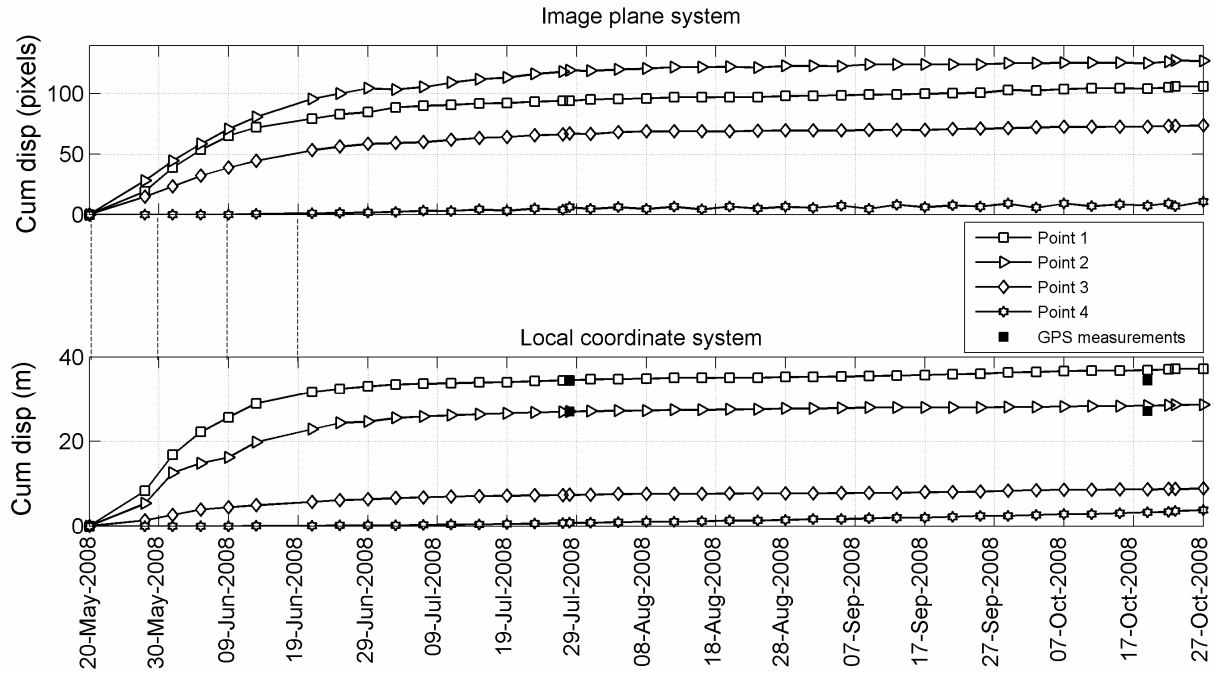

Figure 8. Cumulated displacements of points (1, 2, 3 and 4) located in the upper, medium, lower and stable part of the mudslide in the image plane system and in the local coordinate system in 2008. Their location is shown in Figure 7.

5.2 *Displacement field in the local coordinate system*

The horizontal displacements of the 20th of May corroborate the previous analysis in term of metric displacements. The displacements field varies temporally and spatially. The total amplitude of displacements decreases from the upper part (10.5 m in 4 days) to the lower part of the mudslide (1.1 m in 4 days) as shown by the points 1,2,3 and 4 in Figure 10 in the local coordinate system.

The normal landslide activity is recovered with an average daily velocity of about 0.01 $m.day^{-1}$ between the end of July and October 2008. Horizontal cumulated displacements reach 38 m in the upper part (Points 1, Figure 8) and 7 m in the lower part (Points 3). No significant velocity change is observed during that period.

The accuracy of the converted displacement is assessed by a null test over stable areas. 95 % of the points located in motionless area present a residual displacement less than 0.30 m which is in agreement with the analyses of section §4.2. The global accuracy of the technique is better defined by comparing the displacements obtained with the DIC technique and displacement measured with the DGPS monitoring (Figure 9). The accuracy varies between 10 to 20%. The constant DEM used for the georeferencing and slight movements of the camera are the main causes of the error. When displacements are large, morphologic changes are significant. Consequently, the accuracy of the method decreases.

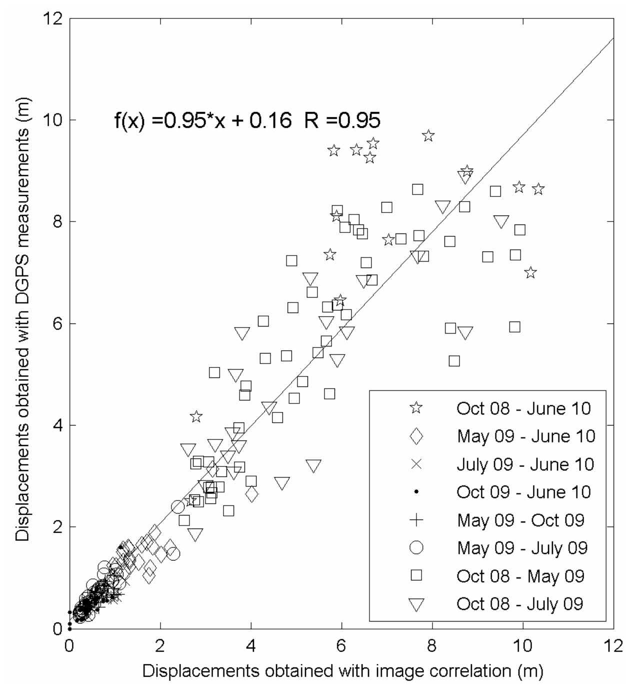

Figure 9. Accuracy and validation of the DIC technique by comparing the displacements obtained with the DIC technique with the displacements obtained with the DGPS monitoring.

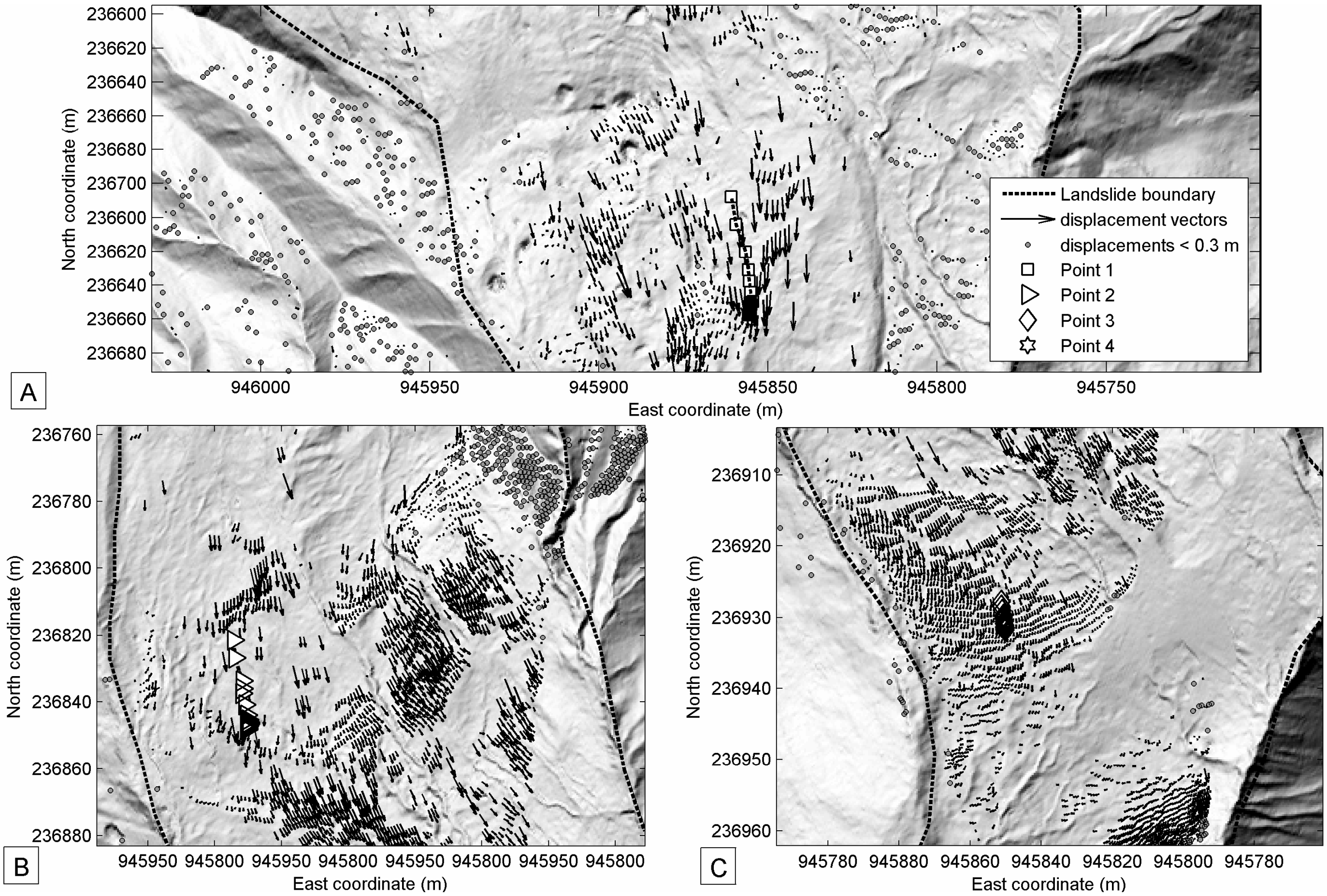

Figure 10. Displacement field for the 20th May 2008 in the local coordinate system in the upper part (A), in the middle part (B) and in the lower part (C) of the mudslide. The trajectories of the points 1, 2, 3 and 4 are also shown. Their cumulated displacements are presented in Figure 8.

6 DISCUSSION AND CONCLUSION

The examples presented in this paper demonstrated the efficiency of the low cost monitoring system based on DIC technique.

If the landslide is mainly translational without excessive changes in elevation, the same DEM can be used to estimate the displacements in the local coordinate system. The accuracy of the converted displacements will obviously depends on the accuracy and the resolution of the DEM. Refining the internal parameters of the camera (eg. radial distortion) might not significantly increase the accuracy because the constant DEM and the slight external parameters changes are the major sources of uncertainties in this method. Acquisitions of several accurate DEMs during the year and a systematic adjustment of the external parameters on fixed control points for each image acquisition would improve the displacement accuracy in the local coordinate system.

Despite its simplicity, the technique is limited by important changes in meteorological conditions (snow, clouds, rain storm), in surface conditions (important ground deformations due to rapid landslides) and in illumination conditions (changes in shadow length and orientation, only operational during the daytime) which drastically affect the correlation accuracy. These aspects have to be taken into account for integrating this technique in an early warning system. Development is also needed for direct data transfer.

ACKNOWLEDGEMENTS

This work was supported by the European Commission within the Marie Curie Research and Training Network '*Mountain Risks: from prediction to management and governance*' (2007-2010, Contract MCRTN-035798). The authors would like to acknowledge Andre Stumpf (Faculty of Geo-Information Science and Earth Observation, Netherlands) and Sabrina Rothmund for their help on the field. The authors thank Dr. Supper (Geological society of Austria) for his help in improving the manuscript.

REFERENCES

Bastard M., 2009. Caractérisation de la cinématique de glissement de terrain par technique de correlation d'image optique. Master thesis. University of Strasbourg (EOST). Institut de Physique du Globe, Strasbourg, France.

Cardenal J., Mata E., Perez-Garcia J.L., Delgado J., Andez M.A., Gonzalez a., Diaz-de-Teran J.R. 2008. Close Range Digital Photogrammetry Techniques applied to Landslide Monitoring. International Archives of the Photogrammetry, *Remote sensing and Spatial Information Sciences*. Vol XXXVII. Part B8.

Casson B., Baratoux D., Delacourt C., Allemand P. 2003. La Clapière" landslide motion observed from aerial differential high resolution DEM. *Engineering Geology*. **68**: 123-139.

Casson B., Delacourt C., Allemand, P. 2005 ; Contribution of multi-temporal sensing images to characterize landslide slip surface – Application to the La Clapière Landslide (France). *Natural Hazards and Earth System Sciences* **5**: 425-437.

Chambon G. 2003. Caractérisation expérimentale du frottement effectif des zones de faille. PHD Thesis. Université Paris XI Orsay, ENPC, pp. 204.

Chambon, G., Schmittbuhl, J., Corfdir, A., Vilotte, J.-P., Roux, S. 2003. Shear with comminution of a granular material: microscopic deformations outside the shear band, *Phys. Rev*. E 68, 011304.

Debella-Gilo M., Kääb A. in press. Sub-pixel precision image matching for measuring surface displacements on mass movements using normalized cross-correlation. *Remote Sensing of Environment*.

Delacourt, C., Allemand P., Casson B., Vadon H. 2004. Velocity field of the "La Clapiere" landslide measured by the correlation of aerial and Quick-Bird satellite images, *Geophys. Res. Lett*. **31**: 1-5.

Delacourt, C., Allemand, P., Berthier, E., Raucoules, D., Casson, B., Grandjean, P., Pambrun, C., Varel, E. 2007. Remote-sensing techniques for analysing landslide kinematics: a review. *Bulletin de Société Géologique* **178**: 89-100.

Fisher, P.F., 1991. First experiments in viewshed uncertainty: The accuracy of the viewshed area. *Photogrammetric Engineering Remote Sensing*, **57**: 1321-1327.

Franklin, W.R., and C.K. Rav, 1994. Higher isn't necessarily better: Visibility algorithms and experiments, Proceedings of-the 6th International Symposium on Spatial Data Handling, Edinburgh, Scotland **2**: 751-770.

Heikkila J. and Silven O. 1997. A four-step camera calibration procedure with implicit image correction. *IEEE Comput. Soc*: 1106-1112.

Hilds F., 2003. Mesure de champs de déplacement par corrélation d'images et applications en mécanique des solides, Notes de cours IPSI. Laboratoire de Mécanique et Technologie, CNRS-UMR 8535, Université Paris 6, France.

Kääb, A. 2002. Monitoring high-mountain terrain deformation from repeated air- and spaceborne optical data: Examples using digital aerial imagery and ASTER data, *J. Photogramm. Remote Sens.*, **57**(1-2): 39–52.

LePrince S., Berthier E., Ayoub F., Delacourt C., Avouac J.-P. 2008. Monitoring Earth Surface Dynamics With Optical Imagery. *Eos* **89** (1): 1-5.

Lewis, J.P., 1995. Fast normalized cross-correlation, *Vision Interface*: 120-123.

Malet, J.-P., Maquaire, O., Calais, E. 2002. The use of Global Positioning System for the continuous monitoring of landslides. Application to the Super- Sauze earthflow (Alpes-de-Haute-Provence, France). *Geomorphology*, **43**: 33-54.

Mikhail, E., Bethel, J. S., and McGlone, J. C. 2001: Introduction to Modern Photogrammetry, Hardcover edition, New-York, 479.

Press, W. H., B. P. Flannery, S. A. Teukolsky, et W. T. Vetterling. 1997. Numerical Recipes in C, The Art of Scientific Computing, Second Edition, Cambridge Univ. Press, New York.

Travelletti J. & Malet J-P. Characterization of the 3D geometry of flow-like landslides: a methodology based on the integration of multi-source data. *Submitted in Engineering Geology*.